DEVELOPMENT OF EMITTANCE METER INSTRUMENT FOR MYRRHA

A. R. Páramo[†], I. Bustinduy, S. Masa, R. Miracoli, V. Toyos, S. Varnasseri
Consorcio ESS-Bilbao, Spain
F. Doucet, L. de Keukeleere, A. Ponton, A. Tanquintic, SCK-CEN, Belgium
J. Herranz, ProActive R&D, Spain

Abstract

For the commissioning of the MYRRHA proton Linac an Emittance Meter Instrument (EMI) has been foreseen. The EMI will be installed in a dedicated test bench for linac commissioning. The test bench will be initially placed after the RFQ with energies of 1.5 MeV, and in later stages moved to other sections of the Normal Conducting Linac for operation at 6 and 17 MeV.

The MYRRHA EMI is composed of two slit and grid subsystems for measurement of the phase space in the horizontal and vertical directions. For collimating the beam, graphite slits are used, and the beam aperture is measured in the SEM grids placed downstream. The control system performs signal amplification, data acquisition, and motion control, with the different systems integrated in an EPICs IOC.

The system, manufactured by ESS-Bilbao and Proactive R&D, has been tested on the ESS-Bilbao 45 keV and soon will be integrated in MYRRHA facilities. We present the EMI design, with irradiation analysis and emittance reconstruction, and the integration tests results.

INTRODUCTION

The MYRRHA project aims for the development of accelerator driven subcritical fission reactor. The current phase of the project, named MINERVA, will realise a 100 MeV, 4 mA superconducting linac. A prototyping of the normal conducting MINERVA injector is ongoing at SCK CEN in Belgium [1]. Currently commissioning of RFQ and Normal-Conducting Linac is in progress. For characterization of beam emittance and phase-space the Emittance Meter (EMI) has been developed. The EMI will be installed in a test bench used for Linac commissioning at different energies, 1.5, 6 and 17 MeV (see Table 1).

Table 1: Main Design Parameters for MYRRHA EMI

Parameter	Value
Current	4 mA
Pulse duration	100 μs
Freq.	10 Hz
Duty Cycle	0.1 %
Minimum Beam Size, rms	1 mm
Max. Beam Extension	± 20 mm
Max. Beam Divergence	± 20 mrad
Beam Energy	1.5 / 6 / 17 MeV
Beam Power	6 / 24 / 68 kW
Average Power	6 / 24 / 68 W

The MYRRHA EMI is developed with a similar design as the ESS MEBT Emittance Meter [2]. The EMI is based on a slit/grid system (see Figure 1). For measuring the phase-space the beam is sliced in the slit, getting the beam position. Then downstream the beam opens and with the signal measured in the grid the beam divergence is estimated. By performing the operation for different slit and grid positions the emittance can be reconstructed.

We have performed validation that the emittance meter can be operated under the irradiation conditions expected in MYRRHA. For the slit graphite blades have been chosen to withstand beam irradiation with a slit aperture of 100 μm. After the slit a grid is placed. The grid is composed of 16 tungsten wires of ϕ35 μm and separated 500 μm. The grid is enclosed between two bias plates allowing for effective suppression of secondary electrons. When positive bias voltages are applied the secondary electrons emitted in the tungsten wires are attracted by the bias plates and leave the grid.
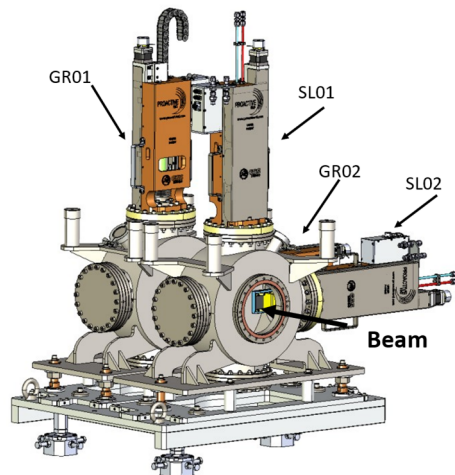

Figure 1: MYRRHA EMI assembly with slit & grids in the x/y planes.

EMI DESIGN

To characterize the performance of the EMI, we have studied the expected emittance, from the Tracewin source term we perform slit/grid simulations using linear particle tracing with python scripts, comparing the reconstructed emittance to the source values.

In Figure 2 we show a simulation at 1.5 MeV, for an emittance scan of 29 slit positions from -7 mm to +7mm of the beam centre, and a grid with an aperture of ±3.75 mm or ±10 mrad (16 wires separated 0.5 mm for a slit grid distance of 350 mm). The analysis of emittance reconstruction

---

† arparamo@essbilbao.org

shows that under ideal conditions the reconstructed emittance is similar to the source term and can be kept in a range of ~1%. Apart from the reconstruction effect, there can be emittance errors due to the effect of signal noises or position incertitude, in total we aim for a total emittance error below 10%.
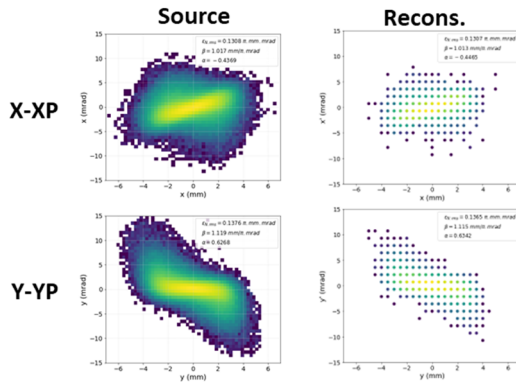

Figure 2: Tracewin source term (left) and simulated emittance reconstruction (right) for 1.5 MeV.

Due to the high currents, energy and small beam sizes the EMI can only be used with short beam pulses, being the design conditions pulses of 100 μs at 10 Hz.

In the slit, the energy deposited by ion irradiation leads to the appearance of thermomechanical stresses. We estimate the irradiation stopping power using SRIM, and the thermomechanical response using FENICs. For the geometry we use a 1D model with 3 mm of thickness with a mesh size of 1 μm and pulses of 100 μs.

In Figure 3, we show the temperature and stresses increase in the irradiated graphite slit during an irradiation pulse. The temperature increase is ~600 K with stresses of ~40 MPa. For different beam energies (1.5-17 MeV) the values are similar, since although the stopping power is higher for lower beam energies, the shallower deposition helps heat diffusion lowering the temperature increase. In all cases the stresses are below the compressive strength of graphite (~130 MPa [4]), and graphite slits could be considered for the MYRRHA Emittance Meter.
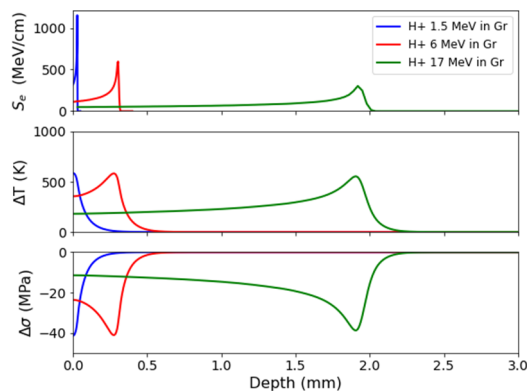

Figure 3: Stopping Power (top), temperatures (middle) and stresses (bottom) increase during irradiation.

For the SEM Grid it is required to operate below thermionic emission limits, which is attained operating with tungsten wires temperature below 2000 K [5]. The wire heating can be estimated by solving the heat equation:

$$\frac{dT}{dt} = \frac{S_e \cdot I''}{\rho \cdot c_p} - \sigma_{SB} \cdot \epsilon \cdot \frac{A}{V} \cdot \frac{T^4 - T_0^4}{\rho \cdot c_p} \qquad (1)$$

where T is the wire temperature, t the time, S_e the average stopping power in the wire, ρ the material density, c_p the material heat capacity, σ_{SB} the Stefan Boltzmann constant, ϵ the material emissivity, A the wire area and V the wire volume, $(A/V=2/r)$, and I'' the beam current flux, for calculations we assume a current flux of 40 A/m^2 estimated from beam simulation after the slit.

In Figure 4 we show the wire heating for the different scenarios, in all cases the temperature is below 2000 K.
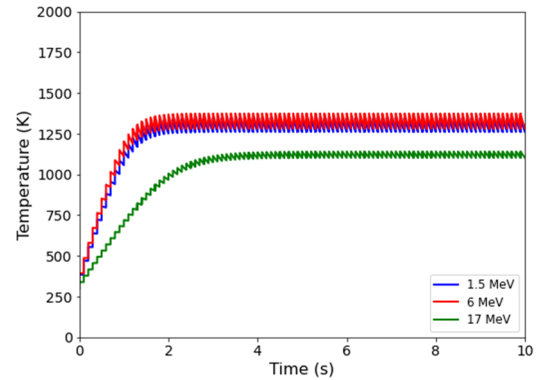

Figure 4: Wire temperature evolution for 1.5, 6 and 17 MeV proton irradiation.

EMI CONTROL & ELECTRONICS

The EMI control system is composed of different systems (see Figure 5): with a Front-End for signal amplification, power supply for bias voltage, I/O, motion control and DAQ systems. The control hardware is integrated in modules for its installation a 19" rack of the MYRRHA gallery. The control software is developed in EPICs.

The Front-End design is based on the ESS EMU MEBT Front End design [6]. The Front-End is composed of Trans-Impedance Amplifiers (TIA) plus a variable gain amplifier. In the Front-End, the TIA stage has a fix gain of 10 000 V/A, and the gain amplifier a variable gain of 1-100. For SEM Grid bias voltage two ±1 kV Iseg DPR bipolar power supplies are included. For I/O and motion control a subrack with Beckhoff modules is used. For motion control EL7047 modules are used for stepper motors drivers, EL5101 for the encoder, and digital I/O modules for limit switches. For the DAQ system we use PXI systems from National Instruments, with a PXIe-1071 chassis, PXIe 8840 controller and PXIe-6349 acquisition card with 32 differential channels with 16 Bits, 500 kSPS simultaneous acquisition. The acquisition is controlled with Labview and variables published in EPICs using Labview EPICs IOC.

For integration of the control system an EPICs IOC is developed. The IOC includes PVs for communication with Beckhoff IOC modules using ethercat with ECMC libraries [7], acquisition PVs for communication with PXI DAQ

31st Int. Linear Accel. Conf.   LINAC2022, Liverpool, UK   JACoW Publishing

ISBN: 978-3-95450-215-8   ISSN: 2226-0366   doi:10.18429/JACoW-LINAC2022-TUPOJO12

using channel access and PVs for scanning and postprocessing functionalities. he EPICs IOCs is installed in a Beckhoff C6030 CPU over a at Centos7 OS and the control GUIs implemented in CSS. For the emittance scan the sequence is implemented using pyepics and the results saved in hdf5 format for postprocessing.
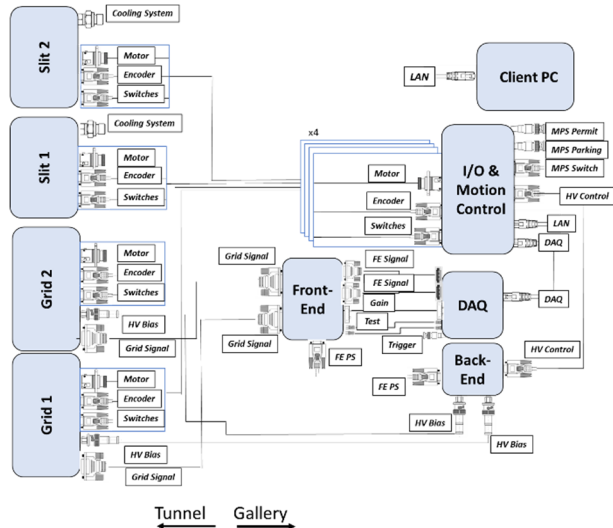

Figure 5: Schematic of the different systems for the EMI.

ESS-BILBAO INTEGRATION TEST

For the verification of the different systems an integration tests of the MYRRHA EMI was performed in ESS-Bilbao. The test included assembly of the EMI after the ESS-Bilbao LEBT for operation with the ESS-Bilbao 45 kV beam (see Figure 6). The ESS-Bilbao injector is composed by an ion source (ISHP) and the LEBT [8]. In the LEBT there are two solenoids, two ACCTs, and a φ5 mm retractile collimator at the LEBT entrance.
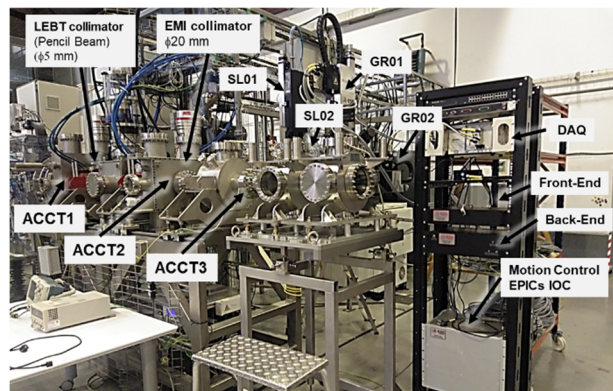

Figure 6: Configuration of the ESS-Bilbao LEBT & MYRRHA EMI for tests.

For beam tests we operated with a pencil beam using a φ5 mm retractile collimator. The beam extraction is ~30 mA, of which the pencil beam is approximately 0.2 mA in the LEBT and approximately 0.1-0.15 mA at the entrance of the EMU.

To obtain the beam profile we performed a position scan using a PyEpics script. In Figure 7 we observe the beam profile with Grid 01 (y plane). In the beam profile we observe a main peak corresponding to H+, and a secondary pulse to other species (mainly H2+) with larger size, which agrees with previous observations in the ESS-Bilbao LEBT [8].
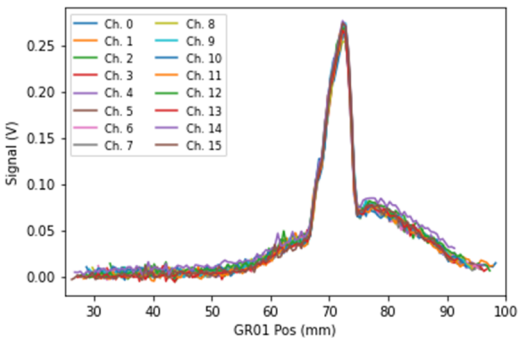

Figure 7: Pencil Beam Profile Scan with Grid 01.

For the emittance scan we first adjusted scanning parametres are adjusted (slit, grid position and resolution) and performed a scanning routine.

In Figure 8 we show the y-y' phase space-after an emittance scan with 29 slit steps from -7 mm to +7 mm (0.5 mm resolution) and 5 grid measurements for a resolution of 0.35 mrad. We observe two ellipses, from the different extracted species (H+, H2+). For adequate emittance calculation it is necessary to discard signal noises outside the beam phase-space. We have compared values of emittance with 0 %, and 2 % (~0 mV, and 20 mV) background subtraction. Observing that when noise signals are removed values of ~0.03 π·mm·mrad for normalized rms emittance. Note that these values should be taken really cautiously, since we are just extracting a pencil beam with several species.
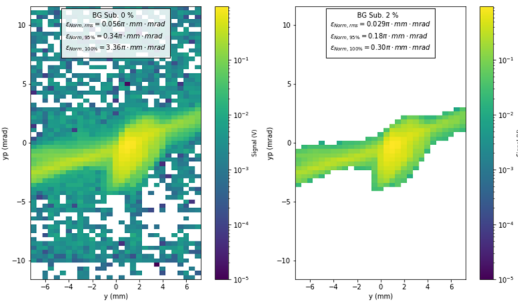

Figure 8: ESS-Bilbao pencil beam phase-space and emittance in y plane for 0%, and 2% background subtraction.

CONCLUSIONS

In this work, we describe the design of the MYRRHA Emittance Meter and its integration test in the ESS-Bilbao LEBT. The Emittance Meter will operate in the MYRRHA Normal Conducting Linac for energies of 1.5-17 MeV using a slit/grid system. For the design of the Emittance Meter we have studied the emittance reconstruction, irradiation effects and developed the integrated system with the electronics and EPICs control.

Finally, we have integrated the EMI and its electronics and control into the ESS-Bilbao injector, observing pencil beam profile and performing emittance scans.

REFERENCES

[1] A. Gatera *et al.*, "MYRRHA-MINERVA injector status and commissioning", in *Proc. HB'21*, Batavia, IL, USA, Oct. 2021, pp. 186-190. `doi:10.18429/JACoW-HB2021-WEBC3`

[2] R. Garoby *et al.*, "The European Spallation Source design", *Phys. Scr.*, vol. 93, no. 1, p. 014001, 2017.

[3] S. Humphries Jr., "Charged particle beams", *Wiley-Interscience; NY, USA.* (849 pages), 1990.

[4] SGL Group: The Carbon Company, "Specialty Graphites for the Metal Industry".

[5] B. Cheymol, "Effects of energy deposition Models and conductive cooling on wire scanner thermal load, analytical and finite element analysis approach", in *Proc. HB'16*, Malmö, Sweden, Jul. 2016, pp. 221-225. `doi:10.18429/JACoW-HB2016-MOPL016`

[6] R. Baron, "24 Channels ESS MEBT EMU Front-End hardware manual", ESS, Internal ESS, Jul. 2020.

[7] T. Gahl *et al.*, "ECMC, the Open Source Motion Control Package for EtherCAT hardware at the ESS", in *Proc. ICALEPCS'17*, Barcelona, Spain, Oct. 2017, pp. 71-75. `doi:10.18429/JACoW-ICALEPCS2017-MOCPL05`

[8] Z. Izaola *et al.*, "Advances in the development of the ESS-Bilbao proton injector", in *Proc. HB'16*, Malmö, Sweden, Jul. 2016, pp. 323--328. `doi:10.18429/JACoW-HB2016-TUPM1Y01`